

# Ultrafast demagnetization in bulk nickel induced by X-ray photons tuned to Ni $M_3$ and $L_3$ absorption edges

Konrad J. Kapcia,<sup>1,2,\*</sup> Victor Tkachenko,<sup>3,2,†</sup> Flavio Capotondi,<sup>4</sup> Alexander Lichtenstein,<sup>3,5</sup> Serguei Molodtsov,<sup>3,6,7</sup> Przemysław Piekarz,<sup>8</sup> and Beata Ziaja<sup>2,8,‡</sup>

<sup>1</sup>*Institute of Spintronics and Quantum Information, Faculty of Physics, Adam Mickiewicz University in Poznań, Uniwersytetu Poznańskiego 2, 61614 Poznań, Poland*

<sup>2</sup>*Center for Free-Electron Laser Science CFEL, Deutsches Elektronen-Synchrotron DESY, Notkestr. 85, 22607 Hamburg, Germany*

<sup>3</sup>*European XFEL GmbH, Holzkoppel 4, 22869 Schenefeld, Germany*

<sup>4</sup>*Elettra-Sincrotrone Trieste S.C.p.A, 34149 Trieste, Basovizza, Italy*

<sup>5</sup>*University of Hamburg, Jungiusstr. 9, 20355 Hamburg, Germany*

<sup>6</sup>*Institute of Experimental Physics, TU Bergakademie Freiberg, Leipziger Strasse 23, 09599 Freiberg, Germany*

<sup>7</sup>*Center for Efficient High Temperature Processes and Materials Conversion (ZeHS), TU Bergakademie Freiberg, Winklerstrasse 5, 09599 Freiberg, Germany*

<sup>8</sup>*Institute of Nuclear Physics, Polish Academy of Sciences, Radzikowskiego 152, 31-342 Kraków, Poland*  
(Dated: July 11, 2023)

Studies of light-induced demagnetization started with the experiment performed by Beaupaire et al. on nickel. Here, we present theoretical predictions for X-ray induced demagnetization of nickel, with X-ray photon energies tuned to its  $M_3$  and  $L_3$  absorption edges. We show that the specific feature in the density of states of the d-band of Ni, a sharp peak located just above the Fermi level, strongly influences the change of the predicted magnetic signal, making it stronger than in the previously studied case of cobalt. We believe that this finding will inspire future experiments investigating magnetic processes in X-ray irradiated nickel.

## I. INTRODUCTION

Ultrafast control of magnetization with lasers remains a hot topic in laser and solid-state physics communities. Apart from traditional terahertz and optical lasers, the state-of-art XUV or X-ray free-electron lasers [1–5] are now also used for demagnetization studies. The main advantage of these lasers is possibility to resonantly excite core electrons to the magnetically sensitive d-band. As the electronic occupation in the the d-band determines the magnetization of the material, the X-ray induced electronic excitation changes the population of spin-up and spin-down electrons in the band. This results in the decrease of the total magnetic moment in the material [6–8]. In our previous studies [6, 7], we modeled the experimentally observed ultrafast decrease of the X-ray scattering signal from X-ray irradiated cobalt which reflected a transient decrease of the cobalt magnetic moment. The XSPIN simulation tool was developed to follow the progressing demagnetization of cobalt. Our studies have shown that the signal decrease can be explained by ultrafast electron-driven demagnetization.

In this paper, we will apply our model to another widely-used magnetic material, nickel. Magnetic moments of nickel and cobalt are  $0.66 \mu_B$  and  $1.70 \mu_B$  respectively [9]. As nickel’s Curie temperature (627 K)

[10] strongly differs from that of cobalt (1400 K), such study can reveal a potential effect of the Curie temperature on the demagnetization dynamics. Laser triggered demagnetization of nickel has been studied in various papers, see, e.g., [11–15]. Interestingly, so far, we have not found any relevant experimental data on Ni demagnetization recorded at XFEL facilities. Therefore, the actual comparison between Co and Ni demagnetization will be performed with theoretical predictions only.

### A. Simulation scheme

As in our previous works [6–8], we will use our recently developed XSPIN code to obtain predictions for the ‘magnetic signal’ from the X-ray irradiated nickel. The electronic density of states is obtained from the density functional theory (DFT) calculations implemented in the Vienna Ab initio Simulation Package (VASP) [16–18]. Average absorbed doses considered in the simulations are chosen not to cause structural changes (atomic dislocations) in the irradiated materials. Therefore, the equilibrium density of states (DOS) can be used throughout the whole simulation (the ‘frozen atom’ assumption). The occupations of electronic levels change during the material exposure to the X-ray pulse, as due to the photoionization, impact ionization and Auger process, excited electrons leave the band to the continuum. Later, they relax back to the band. As the electrons are heated up by the pulse, they remain hot on femtosecond timescales considered in this study, as their temperature can only decrease through an exchange with the lattice which follows on longer ((sub)ps) timescales. Moreover,

\* e-mail: [konrad.kapcia@amu.edu.pl](mailto:konrad.kapcia@amu.edu.pl); ORCID ID: [0000-0001-8842-1886](https://orcid.org/0000-0001-8842-1886)

† e-mail: [victor.tkachenko@xfel.eu](mailto:victor.tkachenko@xfel.eu); ORCID ID: [0000-0002-0245-145X](https://orcid.org/0000-0002-0245-145X)

‡ e-mail: [ziaja@mail.desy.de](mailto:ziaja@mail.desy.de); ORCID ID: [0000-0003-0172-0731](https://orcid.org/0000-0003-0172-0731)

due to the assumed common thermalization of all electrons, both spin-up and spin-down ones (following Fermi Dirac distribution with a common temperature and a chemical potential), the numbers of spin-up and spin-down electrons will be different from the corresponding values in the initial state. This thermalization-induced spin flip process, changing the population of spin-up and spin-down electrons, leads to a change of the magnetic signal.

For the simulation, we use a simulation box with  $N = 512$  Ni atoms. We provide averaging over 100 000 realizations in the Monte Carlo module. The XFEL pulse is assumed to have a Gaussian temporal profile of the duration of 70 fs FWHM (full width at half maximum) for M-edge case ( $M_3 = 66.2$  eV) and 50 fs FWHM for L-edge case ( $L_3 = 852.7$  eV). The pulse duration was chosen such to compare the XSPIN predictions for nickel with our previous results for cobalt presented in [6–8]. For more details on the simulation parameters, see Tab. I.

## II. RESULTS

### A. Spin-polarized electronic density of states from density functional theory calculations

In order to obtain spin-polarized electronic density of states for bulk nickel, we performed first-principle calculation, using the projector augmented wave (PAW) potentials [19] and the generalized gradient approximation (GGA) in the Perdew, Burke, and Ernzerhof (PBE) parametrization [20], implemented in the VASP code [16–18].

For the summation over the reciprocal space, we used  $27 \times 27 \times 27$  Monkhorst-Pack  $k$ -point grid [21]. The spin-polarized density of states for fcc bulk Ni (calculated for the experimental bulk value of the lattice constant,  $a = 3.524$  Å) is presented in Figure 1. It is in an agreement with other DFT calculations (see also, e.g., [22]). For comparison, the density of states for fcc bulk Co (with  $a = 3.545$  Å [23]) used in Refs. [6, 7] is also presented. The calculated magnetic moments of nickel and cobalt are  $0.62 \mu_B$  and  $1.61 \mu_B$ , respectively i.e., with a good agreement with those from [9].

### B. Electronic properties of X-ray irradiated nickel

Below we present the results on the transient distributions of excited electrons and holes obtained with the XSPIN code for nickel and for cobalt (cf. also [6, 7]) irradiated with X rays tuned to their M absorption edges ( $\sim 67$  eV and  $\sim 61$  eV respectively). Figure 2 shows: (a) the transient number of polarized high energy electrons (with energies  $> 15$  eV), (b) the number of low energy electrons (with energies  $< 15$  eV), (c) the transient number of deep shell holes (with indicated polarization of

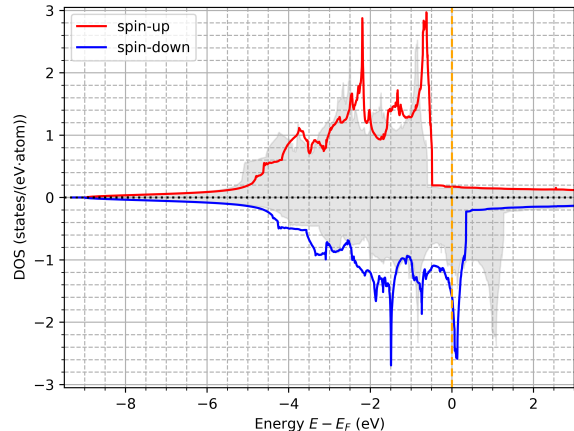


Figure 1. Calculated density of states (states per eV, per atom) for fcc nickel. The red and blue lines correspond to DOS for spin-up and spin-down electrons. The grey shadowed area indicates the density of states for fcc cobalt investigated in Refs. [6–8].

electrons previously occupying the holes), and (d) electronic temperature. The photoexcitation dynamics in Co and Ni look qualitatively similar, with a stronger excitation in Co (Figure 2a-b) than in Ni. Collisional relaxation in Ni is also weaker than in Co (Figure 2c), which leads to the higher electronic temperature in Ni, when compared to Co (Figure 2d).

### C. Generalized transient magnetization

In order to follow changing magnetic properties of irradiated materials, we have introduced in [6] a generalized transient magnetization which reflects the disparity between electronic populations in spin-up and spin-down electronic subsystems in the  $d$ -band:

$$M(t) = \sum_{\hbar\omega_0 - \Delta}^{\hbar\omega_0 + \Delta} [N_{\uparrow}^h(E_{i,\uparrow}) - N_{\downarrow}^h(E_{i,\downarrow})], \quad (1)$$

The probed region in  $d$ -band extends between  $\hbar\omega_0 - \Delta$  and  $\hbar\omega_0 + \Delta$ , where  $\hbar\omega_0 = \hbar\omega_\gamma - E_{\text{edge}}$ . Here,  $\hbar\omega_\gamma$  is the incoming photon energy, and  $E_{\text{edge}}$  is the energy of the resonant core  $p$ -level. The summation goes here over discrete levels. Note that we neglect the subleading effect of the different coupling of polarized light to spin-up and spin-down electrons (XMCD) here. Electronic populations are calculated, assuming Fermi-Dirac distribution of electrons. Knowing at every time step  $t$  electronic temperature  $T_e$  and electronic chemical potential  $\mu$ , we have  $N_{\sigma}^h(E) = 1 - N_{e,\sigma}^{\text{low}}(E)$  and  $N_{e,\sigma}^{\text{low}}(E) = \{1 + \exp[(E - \mu)/k_B T_e]\}^{-1}$ .

Time evolution of squared generalized magnetization  $M^2(t)$  (normalized to its initial value before the pulse

Table I. Simulation parameters used in the present work. All energies are in electronvolts (eV).

Region	Photon energy $\hbar\omega_\gamma$	Probed level $\hbar\omega_0$	$\Delta$	Energy range $[\hbar\omega_0 - \Delta; \hbar\omega_0 + \Delta]$
M-edge	67	0.8	0.7	$[-0.1; 1.5]$
M-edge	68	1.8	0.7	$[1.1; 2.5]$
L-edge	853	0.3	1.0	$[-0.7; 1.3]$
L-edge	854	1.3	1.0	$[0.3; 2.3]$

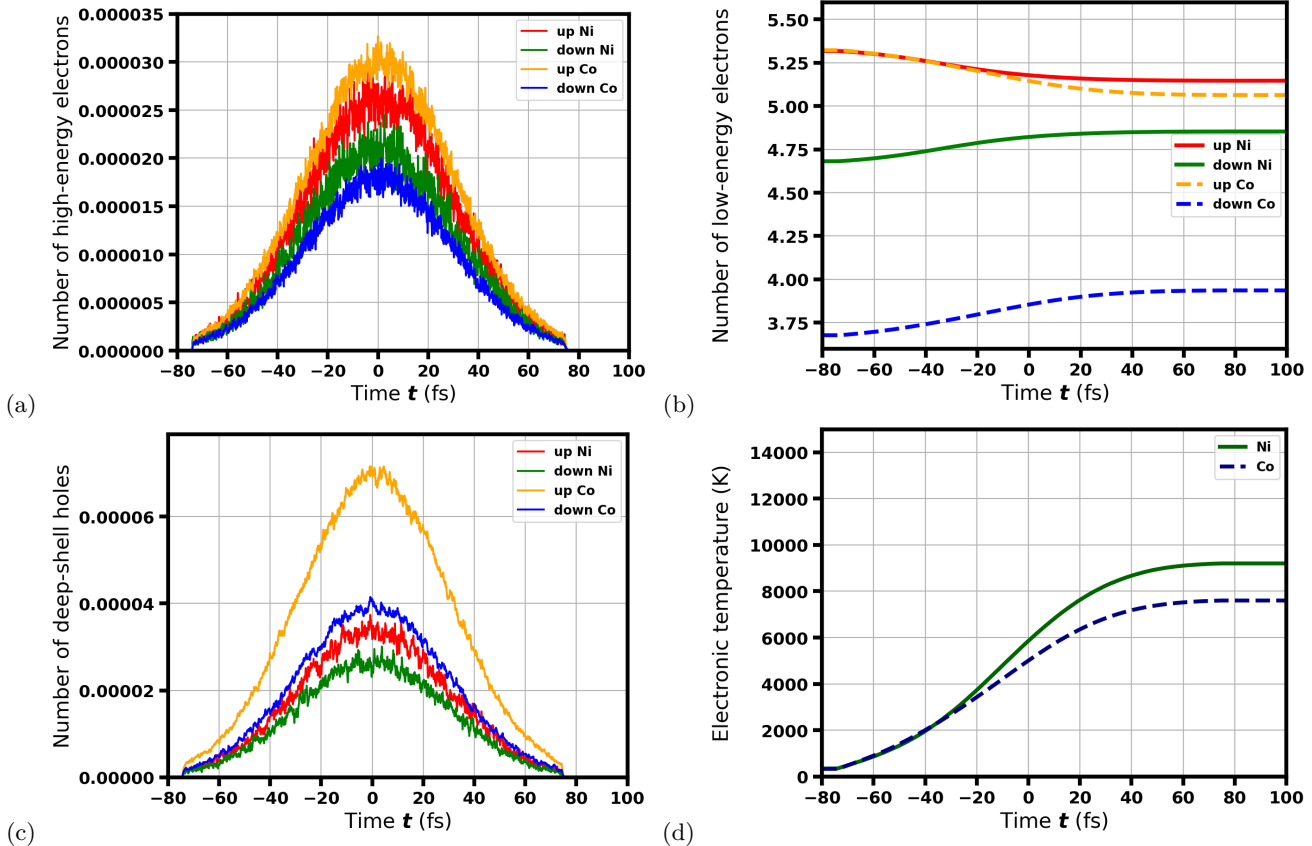


Figure 2. Transient distributions of excited electrons and holes obtained with XSPIN code for X-ray irradiated nickel and for cobalt: (a) the transient number of polarized high energy electrons (with energies  $> 15$  eV), (b) the number of low energy electrons (with energies  $< 15$  eV), (c) the transient number of deep shell holes (with indicated polarization of electrons previously occupying the holes), and (d) electronic temperature. The X-ray photon energy was tuned to M-edge of Ni (67 eV) and to M-edge of Co (61.1 eV). Pulse duration was 70 fs FWHM. Average absorbed dose was 0.93 eV/atom.

at  $t \rightarrow -\infty$ ; cf. also (1)) for different absorbed doses is presented in Figures 3 and 4. The values of  $\Delta$  in Ni were taken from experimental measurements. They are:  $\Delta = 0.7$  eV for nickel M-edge [24–26] and  $\Delta = 1.0$  eV for nickel L-edge [27–30]. One can see that the decrease of magnetization becomes stronger with the increasing absorbed dose, and also strongly changes with incoming photon energy around the absorption edge. Interestingly, if the probed region in d-band includes the sharp peak in the DOS of spin-down electrons near the Fermi level (X-ray photon energies of 67 eV and 853 eV for M- and L-edge respectively; see Tab. I), the observed magnetization change is much stronger than in case when this peak is not included (X-ray photon energies of 68 eV and 854

eV for M- and L-edge respectively). The reason is that the peak ”provides” a large number of unoccupied states for the resonant excitation from p-level, which leads to a stronger decrease of the transient magnetization. Note that the decrease of magnetization is stronger for Ni than for Co (cf. Figure 4 from Ref. [6] and Figure 3 from Ref. [7] at the absorbed dose of 0.93 eV/atom). The reason is that cobalt DOS does not show such a peak close to the Fermi level, and the reduction of magnetization is, therefore, suppressed. This can also explain the lower Curie temperature for nickel than for cobalt.

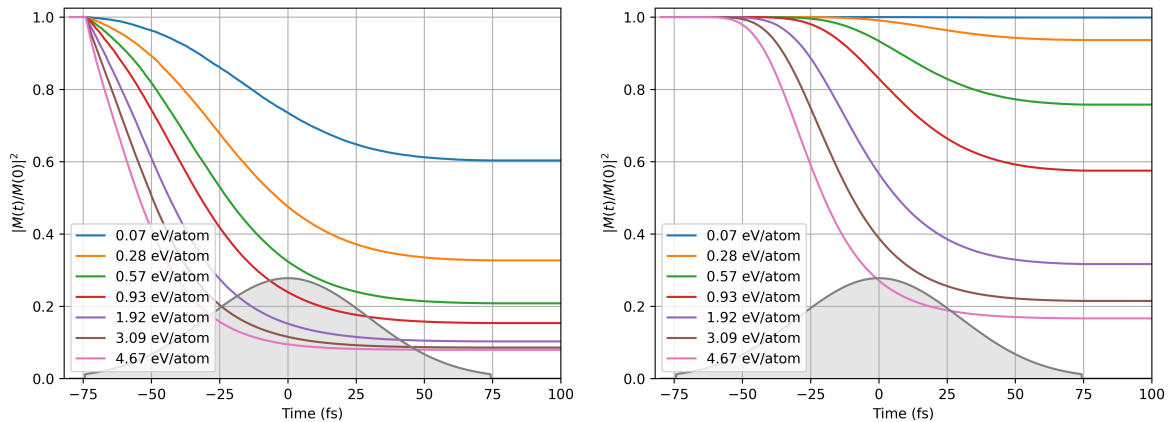


Figure 3. Time dependence of squared normalized magnetization in bulk nickel obtained for the incoming photon energies around the  $M_3$ -edge case of Ni: 67 eV (left) and 68 eV (right). The curves obtained for different average absorbed doses are shown. The  $\Delta$  was equal to 0.7 eV.

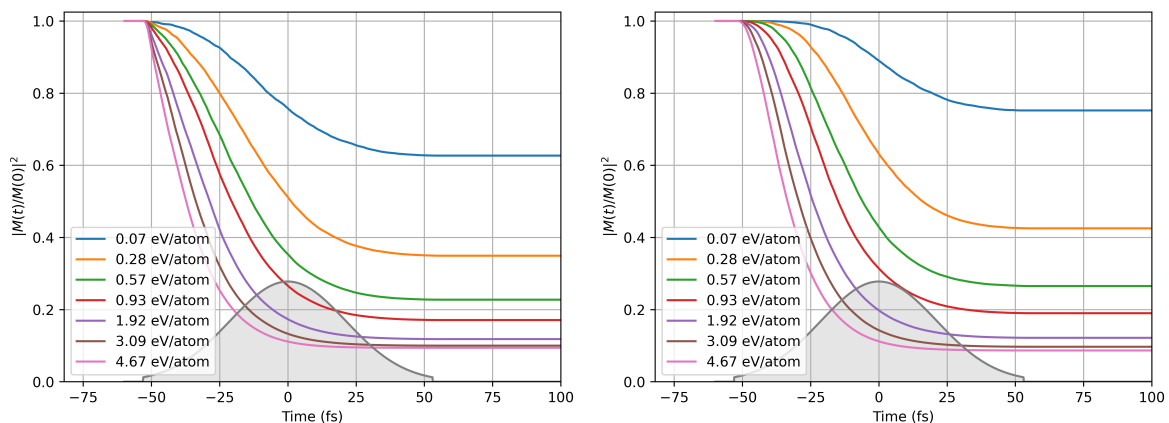


Figure 4. Time dependence of squared normalized magnetization in bulk nickel obtained for the incoming photon energy around the  $L_3$ -edge case of Ni: 853 eV (left) and 854 eV (right). The curves obtained for different average absorbed doses are shown. The  $\Delta$  was equal to 1.0 eV.

#### D. Calculation of the mSAXS signal

Similarly as in [6], we can calculate the mSAXS signal strength from the generalized magnetization. It is obtained as:

$$S = a \int M^2(t)I(t)dt, \quad (2)$$

where  $I(t)$  is the X-ray pulse intensity and  $a$  is a proportionality coefficient. Pulse fluence is then:  $F = \int I(t)dt$ . It is proportional to absorbed dose,  $D \propto F$ , where the proportionality coefficient depends on the material parameters as well as on the photon energy. The dose dependence of the normalized signal strength,  $S_{norm} = S(D)[D_0/S(D_0)]$  for the corresponding experimental  $\Delta$  values is presented in Figure 5. The normalization follows Ref. [6], with the reference dose,  $D_0 = 10^{-4}$  eV/atom for all considered cases.

Similarly as observed for generalized magnetization, the signal strength strongly depends on the fact if the probed region in d-band includes or does not include the sharp peak in the DOS of spin-down electrons near the Fermi level - being distinctly higher in the latter case. This explains also a stronger decrease of  $S_{norm}$  for nickel than for cobalt.

### III. CONCLUSIONS

We provided theory predictions for electronic properties of X-ray irradiated Ni at photon energies close to  $M_3$  or  $L_3$  absorption edge, as well as for the resulting magnetization change and the mSAXS scattering strength. The results obtained indicate the same ultrafast demagnetization mechanism (caused by electronic excitation and relaxation) as in cobalt, occurring at a similar timescale.

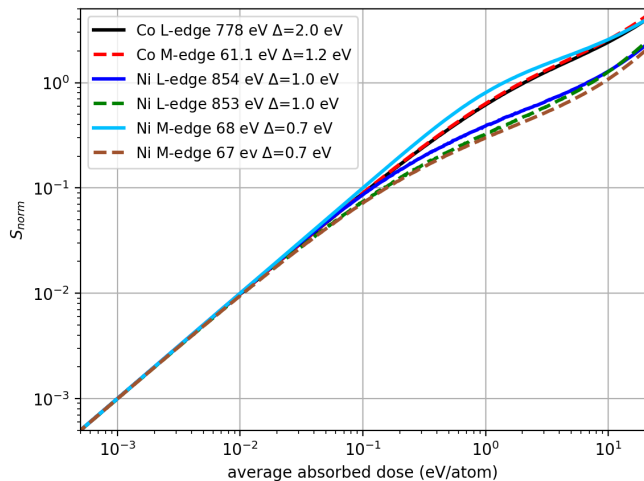


Figure 5. Scattering efficiency  $S_{\text{norm}}$  for nickel and for cobalt as a function of average absorbed dose for X-ray photon energies around M and L absorption edges of Ni and Co.

However, due to the difference in the DOS structure of the d-band, the degree of demagnetization for the equivalent dose would be higher in Ni than in Co. This finding is also consistent with the lower Curie temperature for

nickel than for cobalt.

As in our previous studies on Co, we did not consider here atomic motion, and kept electronic band structure unchanged. This assumption does not hold for the case of high absorbed doses which may induce ultrafast structural changes in irradiated materials. The model should then be developed further, enabling inclusion of atomic dynamics and of the transient band structure.

Nevertheless, we expect that these theory predictions will inspire experimental studies on ultrafast X-ray induced demagnetization of nickel, a benchmark magnetic material of various applications.

## ACKNOWLEDGMENTS

The authors thank Leonard Müller and Andre Philippi-Kobs for helpful discussions at the early stages of the XSPIN model development. K.J.K. thanks the Polish National Agency for Academic Exchange for funding in the frame of the Bekker program (PPN/BEK/2020/1/00184). V.T., A.L., S.M., B.Z. acknowledge the funding received from the Collaboration Grant of the European XFEL and the Institute of Nuclear Physics, Polish Academy of Sciences.

[1] W. Ackermann, G. Asova, V. Ayvazyan, A. Azima, N. Baboi, J. Bähr, V. Balandin, B. Beutner, A. Brandt, A. Bolzmann, R. Brinkmann, O. I. Brovko, M. Castellano, P. Castro, L. Catani, E. Chiadroni, S. Choroba, A. Cianchi, J. T. Costello, D. Cubaynes, J. Dardis, W. Decking, H. Delsim-Hashemi, A. Delsierieys, G. Di Pirro, M. Dohlus, S. Düsterer, A. Eckhardt, H. T. Edwards, B. Faatz, J. Feldhaus, K. Flöttmann, J. Frisch, L. Fröhlich, T. Garvey, U. Gensch, Ch. Gerth, M. Görler, N. Golubeva, H.-J. Grabosch, M. Grecki, O. Grimm, K. Hacker, U. Hahn, J. H. Han, K. Honkavaara, T. Hott, M. Hüning, Y. Ivanisenko, E. Jaeschke, W. Jalmuzna, T. Jezynski, R. Kammering, V. Katalev, K. Kavanagh, E. T. Kennedy, S. Khodyachykh, K. Klose, V. Kocharyan, M. Körfer, M. Kollwe, W. Koprek, S. Korepanov, D. Kostin, M. Krassilnikov, G. Kube, M. Kuhlmann, C. L. S. Lewis, L. Lilje, T. Limberg, D. Lipka, F. Löhler, H. Luna, M. Luong, M. Martins, M. Meyer, P. Michelato, V. Miltchev, W. D. Möller, L. Monaco, W. F. O. Müller, O. Napieralski, O. Napoly, P. Nicolosi, D. Nölle, T. Nuñez, A. Oepelt, C. Pagani, R. Paparella, N. Pchalek, J. Pedregosa-Gutierrez, B. Petersen, B. Petrosyan, G. Petrosyan, L. Petrosyan, J. Pflüger, E. Plönjes, L. Poletto, K. Pozniak, E. Prat, D. Proch, P. Pucyk, P. Radcliffe, H. Redlin, K. Rehlich, M. Richter, M. Roehrs, J. Roensch, R. Romaniuk, M. Ross, J. Rossbach, V. Rybnikov, M. Sachwitz, E. L. Saldin, W. Sandner, H. Schlarb, B. Schmidt, M. Schmitz, P. Schmüser, J. R. Schneider, E. A. Schneidmiller, S. Schnepf, S. Schreiber, M. Seidel, D. Sertore, A. V. Shabunov, C. Simon, S. Simrock, E. Sombrowski,

A. A. Sorokin, P. Spanknebel, R. Spesyvtsev, L. Staykov, B. Steffen, F. Stephan, F. Stulle, H. Thom, K. Tiedtke, M. Fischer, S. Toleikis, R. Treusch, D. Trines, I. Tsakov, E. Vogel, T. Weiland, H. Weise, M. Wellhöfer, M. Wendt, I. Will, A. Winter, K. Wittenburg, W. Wurth, P. Yeates, M. V. Yurkov, I. Zagorodnov, and K. Zapfe, Operation of a free-electron laser from the extreme ultraviolet to the water window, *Nat. Photonics* **1**, 336 (2007).

[2] E. Allaria, R. Appio, L. Badano, W. A. Barletta, S. Bassanese, S. G. Biedron, A. Borgia, E. Busetto, D. Castronovo, P. Cinquegrana, S. Cleva, D. Cocco, M. Cornacchia, P. Craievich, I. Cudin, G. D’Auria, M. Dal Forno, M. B. Danailov, R. De Monte, G. De Ninno, P. Delgiusto, A. Demidovich, S. D. Mitri, B. Diviacco, A. Fabris, R. Fabris, W. Fawley, M. Ferianis, E. Ferrari, S. Ferry, L. Froehlich, P. Furlan, G. Gaio, F. Gelmetti, L. Giannessi, M. Giannini, R. Gobessi, R. Ivanov, E. Karantzoulis, M. Lonza, A. Lutman, B. Mahieu, M. Milloch, S. V. Milton, M. Musardo, I. Nikolov, S. Noe, F. Parmigiani, G. Penco, M. Petronio, L. Pivetta, M. Predonzani, F. Rossi, L. Rumiz, A. Salom, C. Scafuri, C. Serpico, P. Sigalotti, S. Spampinati, C. Spezzani, M. Svandrlík, C. Svetina, S. Tazzari, M. Trovo, R. Umer, A. Vascotto, M. Veronese, R. Visintini, M. Zaccaria, D. Zangrando, and M. Zangrando, Highly coherent and stable pulses from the FERMI seeded free-electron laser in the extreme ultraviolet, *Nat. Photonics* **6**, 699 (2012).

[3] P. Emma, R. Akre, J. Arthur, R. Bionta, C. Bostedt, J. Bozek, A. Brachmann, P. Bucksbaum, R. Coffee, F.-J. Decker, Y. Ding, D. Dowell, S. Edstrom, A. Fisher, J. Frisch, S. Gilevich, J. Hastings, G. Hays,

- P. Hering, Z. Huang, R. Iverson, H. Loos, M. Messerschmidt, A. Miahnahri, S. Moeller, H.-D. Nuhn, G. Pile, D. Ratner, J. Rzepiela, D. Schultz, T. Smith, P. Stefan, H. Tompkins, J. Turner, J. Welch, W. White, J. Wu, G. Yocky, and J. Galayda, First lasing and operation of an ångstrom-wavelength free-electron laser, *Nat. Photonics* **4**, 641 (2010).
- [4] D. Pile, First light from SACLA, *Nat. Photonics* **5**, 456 (2011).
- [5] H. Weise and W. Decking, Commissioning and first lasing of the european xfel, *Proc. of 38th International Free Electron Laser Conference FEL2017, Santa Fe 2017*, 9 (2017).
- [6] K. Kapcia, V. Tkachenko, F. Capotondi, A. Lichtenstein, S. Molodtsov, L. Müller, A. Philippi-Kobs, P. Piekarz, and B. Ziaja, Modeling of ultrafast x-ray induced magnetization dynamics in magnetic multilayer systems, *npj Comput. Mater.* **8**, 212 (2022).
- [7] K. J. Kapcia, V. Tkachenko, F. Capotondi, A. Lichtenstein, S. Molodtsov, L. Mueller, A. Philippi-Kobs, P. Piekarz, and B. Ziaja, Electronic processes occurring during ultrafast demagnetization of cobalt triggered by x-ray photons tuned to the Co  $L_3$  resonance, *Phys. Rev. B* **107**, 094402 (2023).
- [8] K. J. Kapcia, V. Lipp, V. Tkachenko, and B. Ziaja, Theoretical analysis of x-ray free-electron-laser experimental data using Monte-Carlo and molecular-dynamics based computational tools, in *Reference Module in Chemistry, Molecular Sciences and Chemical Engineering* (Elsevier, 2023).
- [9] J. Meyer, M. Tombers, C. van Wüllen, G. Niedner-Schatteburg, S. Peredkov, W. Eberhardt, M. Neeb, S. Palutke, M. Martins, and W. Wurth, The spin and orbital contributions to the total magnetic moments of free Fe, Co, and Ni clusters, *J. Chem. Phys.* **143**, 104302 (2015).
- [10] B. Chatterjee, Oxidation of iron, cobalt and nickel at the curie temperature, *Solid State Commun.* **27**, 1455 (1978).
- [11] E. Beaurepaire, J.-C. Merle, A. Daunois, and J.-Y. Bigot, Ultrafast spin dynamics in ferromagnetic nickel, *Phys. Rev. Lett.* **76**, 4250 (1996).
- [12] B. Koopmans, M. van Kampen, J. T. Kohlhepp, and W. J. M. de Jonge, Ultrafast magneto-optics in nickel: Magnetism or optics?, *Phys. Rev. Lett.* **85**, 844 (2000).
- [13] C. Stamm, T. Kachel, N. Pontius, R. Mitzner, T. Quast, K. Hollmack, S. Khan, C. Lupulescu, E. F. Aziz, M. Wietstruk, H. A. Dürr, and W. Eberhardt, Femtosecond modification of electron localization and transfer of angular momentum in nickel, *Nat. Mat.* **6**, 740 (2007).
- [14] T. Lojewski, M. F. Elhanoty, L. L. Guyader, O. Grånäs, N. Agarwal, C. Boeglin, R. Carley, A. Castoldi, C. David, C. Deiter, F. Döring, R. Engel, F. Erdinger, H. Fangohr, C. Fiorini, P. Fischer, N. Gerasimova, R. Gort, F. de Groot, K. Hansen, S. Hauf, D. Hickin, M. Izquierdo, B. E. V. Kuiken, Y. Kvashnin, C.-H. Lambert, D. Lomidze, S. Maffessanti, L. Mercadier, G. Mercurio, P. S. Miedema, K. Ollefs, M. Pace, M. Porro, J. Rezvani, B. Rösner, N. Rothenbach, A. Samartsev, A. Scherz, J. Schlappa, C. Stamm, M. Teichmann, P. Thunström, M. Turcato, A. Yaroslavtsev, J. Zhu, M. Beye, H. Wende, U. Bovensiepen, O. Eriksson, and A. Eschenlohr, The interplay of local electron correlations and ultrafast spin dynamics in fcc Ni, *Mater. Res. Lett.* **11**, 655 (2023).
- [15] K. Krieger, J. K. Dewhurst, P. Elliott, S. Sharma, and E. K. U. Gross, Laser-induced demagnetization at ultra-short time scales: Predictions of TDDFT, *J. Chem. Theory Comput.* **11**, 4870 (2015).
- [16] G. Kresse and J. Hafner, Ab initio molecular-dynamics simulation of the liquid-metal–amorphous-semiconductor transition in germanium, *Phys. Rev. B* **49**, 14251 (1994).
- [17] G. Kresse and J. Furthmüller, Efficient iterative schemes for ab initio total-energy calculations using a plane-wave basis set, *Phys. Rev. B* **54**, 11169 (1996).
- [18] G. Kresse and D. Joubert, From ultrasoft pseudopotentials to the projector augmented-wave method, *Phys. Rev. B* **59**, 1758 (1999).
- [19] P. E. Blöchl, Projector augmented-wave method, *Phys. Rev. B* **50**, 17953 (1994).
- [20] J. P. Perdew, K. Burke, and M. Ernzerhof, Generalized gradient approximation made simple, *Phys. Rev. Lett.* **77**, 3865 (1996).
- [21] H. J. Monkhorst and J. D. Pack, Special points for brillouin-zone integrations, *Phys. Rev. B* **13**, 5188 (1976).
- [22] L. S. Abdallah, T. M. Tawalbeh, I. V. Vasiliev, S. Zollner, C. Lavoie, A. Ozcan, and M. Raymond, Optical conductivity of  $Ni_{1-x}Pt_x$  alloys ( $0 < x < 0.25$ ) from 0.76 to 6.6 eV, *AIP Advances* **4**, 017102 (2014).
- [23] W. Wang, Z. Hou, R. Lizárraga, Y. Tian, R. P. Babu, E. Holmström, H. Mao, and H. Larsson, An experimental and theoretical study of duplex fcc+hcp cobalt based entropic alloys, *Acta Materialia* **176**, 11 (2019).
- [24] C. Olson and D. Lynch, Temperature dependence of the  $M_{2,3}$  edge in nickel, *Solid State Commun.* **33**, 849 (1980).
- [25] P. S. Miedema, N. Thielemann-Kühn, I. A. Calafell, C. Schüßler-Langeheine, and M. Beye, Strain analysis from M-edge resonant inelastic x-ray scattering of nickel oxide films, *Phys. Chem. Chem. Phys.* **21**, 21596 (2019).
- [26] H.-T. Chang, A. Guggenmos, S. K. Cushing, Y. Cui, N. U. Din, S. R. Acharya, I. J. Porter, U. Kleineberg, V. Turkowski, T. S. Rahman, D. M. Neumark, and S. R. Leone, Electron thermalization and relaxation in laser-heated nickel by few-femtosecond core-level transient absorption spectroscopy, *Phys. Rev. B* **103**, 064305 (2021).
- [27] Y. Uchimoto, H. Sawada, and T. Yao, Changes in electronic structure by Li ion deintercalation in  $LiNiO_2$  from nickel L-edge and o K-edge XANES, *J. Power Sources* **97-98**, 326 (2001).
- [28] K. Carva, D. Legut, and P. M. Oppeneer, Influence of laser-excited electron distributions on the X-ray magnetic circular dichroism spectra: Implications for femtosecond demagnetization in Ni, *EPL (Europhysics Letters)* **86**, 57002 (2009).
- [29] Y. Ufuktepe, G. Akgül, F. Aksoy, and D. Nordlund, Thickness and angular dependence of the L-edge x-ray absorption of nickel thin films, *X-Ray Spectrometry* **40**, 427 (2011).
- [30] W. Gu, H. Wang, and K. Wang, Nickel L-edge and K-edge x-ray absorption spectroscopy of non-innocent  $Ni[S_2C_2(CF_3)_2]_2^n$  series ( $n = -2, -1, 0$ ): direct probe of nickel fractional oxidation state changes, *Dalton Trans.* **43**, 6406 (2014).